Germanene on single-layer ZnSe substrate
Novel electronic and optical properties

Ye, H.Y.; Hu, F.F.; Tang, H.Y; Yang, L.W.; Chen, X.P.; Wang, L.G.; Zhang, G.Q.

DOI
10.1039/c8cp00870a

Publication date
2018

Document Version
Accepted author manuscript

Published in
Physical Chemistry Chemical Physics

Germanene on single layer ZnSe substrate: Novel electronic and optical properties

H. Y. Ye,[‡ab] F. F. Hu,[‡ab] H. Y. Tang,[‡c] L.W. Yang, [‡d] X. P. Chen, [‡ab] L. G. Wang, [‡d] G.Q. Zhang[‡c]

[a] *Key Laboratory of Optoelectronic Technology & Systems, Education Ministry of China, Chongqing University and College of Optoelectronic Engineering, Chongqing University, 400044 Chongqing, China.*

[b] *College of Optoelectronic Engineering, Chongqing University, Chongqing 400044, China*

[c] *Electronic Components, Technology and Materials, Delft University of Technology, Delft 2628 CD, The Netherlands.*

d State Key Laboratory for Nonferrous Metals and Process, General Research Institute for Nonferrous Metals Beijing, Beijing 100088, China.

These authors contributed equally to this work.

Correspondence authors: X.P. Chen (E-mail: xianpingchen@cqu.edu.cn)

ABSTRACT

In this work, the structural, electronic and optical properties of germanene and ZnSe substrate nanocomposites have been investigated using first-principles calculations. We found that the large direct-gap ZnSe semiconductors and zero-gap germanene form a typical orbital hybridization heterostructure with a strong binding energy, which shows moderate direct bandgap of 0.503 eV in the most stable pattern. Furthermore, the heterostructure experience semiconductor-to-metal bandgap transition when subjected to external out-of-plane electric field. We also found that the external strain and compressing the interlayer distance are two simple ways of tuning the electronic structure. An unexpected indirect-direct band gap transition is also observed in AAII pattern via adjusting the interlayer distance. Quiet interestingly, the calculated results exhibit that the germanene/ZnSe heterobilayers structure has a perfect optical absorption in the solar spectrum, infrared light adsorption and UV light zone, which is superior to the individual ZnSe substrate and germanene. The staggered interfacial gap and the tunable energy band structure via interlayer distance, external electric field and strain, thus, the germanene/ZnSe heterostructure is expected to a promising candidate

for field effect transistors (FETs) and nanoelectronic applications.

1. Introduction

In recent years, two-dimensional (2D) nanomaterials, such as graphene, silicene, germanene and arsenene, have opened up tremendous opportunities and drawn a significant amount of research interest due to their tunable and novel electronic, optical and mechanical properties compared with their bulk counterparts. [1,2,3,4,5] These unique properties make them open up tremendous opportunities for attractive applications in next generation ultrathin, flexible and transparent nanoelectronic devices. [6,7,8] As an analogue of graphene, germanene is a two-dimensional (2D) crystal with a low-buckled honeycomb structure,[9,10,11] which has attracted researchers' great interest due to a great deal of semiconductor devices that based on C, Si, and Ge.[12] Because of the weak π-π interactions and distinct coupling of σ and π bonds between Ge atoms, germanene exhibits some new physical behavior beyond graphene.[9,10,13] However, owing to the lack of a band gap and its low structural stability, which hampers its direct applications in logic and high-performance switching devices. However, pairing with a substrate to form a heterostructure is an effective method to solve the problem of opening a band gap in germanene. For example, the vdW germanene/germanane heterostructure has predicted to open a band gap of 82-120 meV at the Dirac point due to the intrinsic interface dipole.[14] The opened band gap is larger than the van der Waals silicane/silicene heterostructure, which is found to be 44-61 meV.[15] The most fascinating property of germanene is that the strong spin-orbit coupling opened a band gap of 23.9 meV at the Dirac point, which indicates that it will be an ideal quantum spin Hall 2D topological insulator.[16] It is worth noting that the opened band gap of germanene is one magnitude larger than the value of honeycomb lattices of freestanding silicene (1.55 meV), [17] but smaller than the methyl-functionalized stanene (148 meV),[18] the hydrogenated or halogenated stanene monolayers (0.2-0.3 eV)[19], hydrogenated arsenene (193 meV),[20] quantum anomalous Hall insulator Nb_2O_3 monolayer (75

meV),[21] as well as X-decorated plumbene monolayers (PbX; X=H, F, Cl, Br, I) with giant tunable gaps (1.03-1.34 eV).[22]

Recently, Sun and coworkers reported that successfully fabricated free-standing ZnSe nanosheets with four atomic thickness from its bulk zinc-blende structure, which shows a clean surface and honeycomb lattice, possessing a direct band gap of 2.50 eV.[23] The double-layer sheet of ZnSe exhibits an enhanced photocurrent density, ~8 and ~195 times higher than that of ZnSe quantum dots and bulk counterparts, respectively. Some theoretical investigations on single-layer ZnSe demonstrate a stable structure and quantum confinement effect stronger than the experimentally synthesized double-layer counterparts, which exhibits versatile electronic properties and it could be employed as potential photocatalyst for water-splitting by absorbing ultraviolet light. [24,25] Li *et al*. showed that the novel tetragonal ZnSe is the most stable structure based on a global minimum search.[26] Great achievements have been made in previous excellent works on germanene and ZnSe, however, a systematic understanding of composites germanene and ZnSe substrate, focusing on the electronic and optical properties of their heterobilayer structure is still lacking.

In this work, using the van der Waals (vdW) corrected density functional theory (DFT) calculations, we systematically investigate the structural, electronic and optical properties of genmanene/ZnSe heterostructure. The interlayer distance, stacking pattern, binding energy and work function are taken into consideration for evaluating the novel heterobilayer structure. The results demonstrate that the combination of germanene and single-layer ZnSe being able to offer a moderate direct band gap, along with a significantly improved optical properties in the visible light region compared with the individual germanene and single-layer ZnSe. We further calculated the band gap of the composite under external electric field (E-field) and mechanical strain. Most interestingly, the bandgaps of germanene/ZnSe heterobilayer can be linearly changed and the semiconductor-to-metal transition can be realized under both E-field and strain.

Furthermore, compressing the interlayer distance is a simple way of tuning the electronic band. We are optimistic and believe that the superior properties obtained of germanene/ZnSe heterobilayer structure will inspire researchers' interest in performing more experiments in it.

2. Method

All first-principle calculations were performed using the DMol^3 package, on the base of the density functional theory (DFT) [27,28] and the generalized gradient approximation (GGA) with Perdew-Burke-Ernzerhof (PBE) functional [29] was used as the exchange-correlation potential. Double numerical atomic orbital plus polarization (DNP) was chosen as the basis set, with the global orbital cutoff of 5.0 Å. In order to better describe the long-range Waals (vdW) interaction between germanene and single layer ZnSe, the dispersion corrected density functional theory (DFT-D) proposed by Grimme [30,31] was employed. Actually, a primitive cell was used for the investigation in order to obtain more accurate results. The kinetic energy cutoff the plane wave was set to 500 eV. The k-points was set to 15×15×1 for the geometry optimizations and electronic properties calculations. The convergence tolerance of energy, maximum force, and maximum displacement were set to 1.0×10^{-5} Ha, 0.002 Ha Å^{-1} and 0.005 Å, respectively. Periodic boundary conditions were applied in the x- and y- directions. An adequately large 30 Å vacuum region was introduced to eliminate the effect of spurious interaction and artificial dipole moment effects from neighboring cells in the direction normal to the germanene surface (z- direction). Besides, due to the underestimation of PBE functional on the band gaps of semiconductors,[32] the Heyd-Scuseria-Ernzerhof (HSE06) hybrid functional[33] was employed to obtain more accurate electronic band structure. For each heterostructure with various conduction, optical properties were calculated with an energy cutoff of 500 eV, implemented in the CASTEP package under the HSE06 hybrid functional method.[34] The BZ integrations are performed by adopting 8×8×1 Monkhorst-Pack grid considering the limited computational resources.

In order to estimate accurately the interaction between germanene and single-layer ZnSe, the binding energy (E_b) per atom is calculated using the following formula

$$E_b = (E_{total} - E_{ZnSe} - E_{germanene})/N, \qquad (1)$$

where E_{total}, E_{ZnSe}, $E_{germanene}$ are the total energy of the composite, and two individual layers (germanene and ZnSe), respectively. N corresponds to the total number of Ge atoms in the unit cell. The more negative E_b value stands for a stronger interface binding.

To assess the thermal stability of germanene/ZnSe heterobilayers, the ab initio molecular dynamics (AIMD) simulations with GGA-PBE functional were performed by DMol^3 code.[35] A 4×4×1 supercell of germanene/ZnSe heterobilayers was annealed and the temperature was set to 310K. Each MD simulation in NVT ensemble lasted for 5 ps with a time step of 1.0 fs, and the temperature was controlled using the Massive NH method.

To calculate the optical properties, in the visible-ultraviolet spectrum, the frequency-dependent dielectric matrixes are determined by the Fermi golden rule within the dipole approximation. The imaginary part of the dielectric function due to the occupied and unoccupied electric states are performed on the basis of the formula,[36]

$$\varepsilon_2(\omega) = \frac{8\pi^2 e^2}{LAm^2\omega^2} \sum_{c,v} \sum_{K} |\langle \mathrm{v}, K \mid p_\alpha \mid c, K \rangle|^2 \delta(E_c(K) - E_v(K) - \hbar\omega) \qquad (2)$$

where c and v represents the conduction and valance states associated with the energies $E_c(K)$ and $E_v(K)$, delta function δ ensures the conversation of energy, A is the sheet area, L is the vertical height between the sheets in the periodic supercell, $\langle\rangle$ is the momentum transition matrix, e is the charge of electron, m and $\hbar$ are the effective mass and Planck constantly, respectively. The absorption coefficient α can be gained by the following equation [37]:

$$\alpha(\omega) = \sqrt{2}\omega[\sqrt{\varepsilon_1^2(\omega) + \varepsilon_1^2(\omega)} - \varepsilon_1(\omega)]^{1/2} \qquad (3)$$

3. Results and Discussion

In order to obtain a thorough knowledge of germanene/ZnSe heterostructure, we first discuss the geometric and electronic structures of individual ZnSe substrate and

germanene. The ZnSe and germanene are obtained by cleaving the (111) plane of the face-centered cubic (FCC) zinc blend phase of their bulk structures. The geometry optimized single-layer ZnSe has a planar structure and a honeycomb lattice, the nearest Se-Se and Zn-Se distances are 4.008 Å and 2.389 Å, which are very close to the measured distances (4.012 Å and 2.457 Å) in the experiment.[23] The lattice constants of germanene and single-layer ZnSe after structural optimizations are a=b=4.017 Å and a=b=4.060 Å, respectively, which are well consistent with the reported values of 4.061 and 4.070 Å.[25,38] The supercell for the heterobilayer is composed by 2×2 unit cells for germanene and ZnSe with tiny lattice mismatch (1.07%). Moreover, compared with the hybrid systems reported previously, [39,40,41] the calculated lattice constant of the relaxed primitive cell of their composite is 4.010 Å, and thus the compression ratios of lattice constants of ZnSe substrate and germanene are negligible.

For the germanene/ZnSe hybrids, four representative stacking patterns, namely, AAI-, AAII-, ABI-, ABII- stacking were considered, as shown in Fig.1. For AA-stacking, germanene and single-layer ZnSe are matched perfectly without mismatch in the xy plane, whereas for AB-stacking, one Zn or Se atom in the supercell was set to sit on the hollow site above the center of a hexagon of germanene. Pattern II including AAII and ABII we obtained is flip the germanene of pattern I vertically 180°, and leads to a novel heterostructure different from Pattern I. The corresponding relaxed structural parameters for all the heterobilayers are listed in Table 1. It is noted that the buckling height ($\delta_{Zn\text{-}Se}$) of single-layer ZnSe in three patterns (AAII and ABI) significantly increase compared with the initial value of 0.475 Å, while the AAI and ABII decrease the value, suggesting that a slight structural distortion in single-layer ZnSe. However, the buckling heights of the germanene ($\delta_{Ge\text{-}Ge}$) in AAII patterns is larger than the individual freestanding one (0.875 Å), while for other three types is lower than that of individual germanene.

From Table 1, it is found that the binding energy (E_b) of these bilayers vary from

-0.093 eV to -0.321 eV per atom with four different stacking orders. It is obvious that the binding energy is independent of the stacking pattern. The interlayer distance *d* follows the order of AAII (2.026 Å) <ABII (2.746 Å)<ABI (2.985 Å)<AAI (3.338 Å), which corresponds to the E_b. It is noted that the interlayer distance of AAii-stacking is 2.026 Å, which is smaller than both the sum of covalent radii of Ge-Zn (2.39 Å) and Ge-Se (2.37 Å), suggesting some covalent bonds may be formed between germanene and ZnSe layers. Furthermore, the calculated binding energy for AAII pattern amounts to 0.321 eV, which is significantly higher than the binding energy of weak vdW interactions, indicating that germanene and ZnSe substrate bounded to each other via other mechanism, such as orbital hybridization or electrostatic interaction. In contrast, for the AAI, ABI and ABII patterns, their interlayer distances are much larger than both bond lengths of Ge-Zn and Ge-Se, indicating that the interaction between germanene and ZnSe layer is the weak vdW interaction. According to the calculated electronic properties, it is found that the opened band gaps exhibit various responses to different stacking patterns. Among the stacking patterns, the AAii-stacking produces a moderate direct band gap of 0.503 eV, accompanied with the minimum interlayer distance and highest binding energy. Considering the interlayer distances and binding energies listed in Table 1, in the following calculations, we mainly focus on the AAii-stacking.

Table 1 Structure/electronic properties of germanene/ZnSe bilayer with different patterns, including the distance between upper ZnSe plane and lower Ge atom (*d*), amplitude of the buckling of Ge ($\delta_{Ge\text{-}Ge}$)and ZnSe ($\delta_{Zn\text{-}Se}$) superlattice, binding energy (E_b), Hirshfeld charge transfer (Q) and energy band gap (E_g). The negative *Q* denotes that the charges transfer from single-layer ZnSe to germanene.

Model	*d* (Å)	$\delta_{Ge\text{-}Ge}$	$\delta_{Zn\text{-}Se}$	E_b (eV)	*Q* (e)	E_g *(eV)*
AAI	3.338	0.706	0.430	-0.093	-0.009	0.287
AAII	2.026	0.927	0.876	-0.321	-0.036	0.503
ABI	2.985	0.712	0.433	-0.151	-0.019	0.053

ABII	2.746	0.623	0.480	-0.160	-0.015	0.249

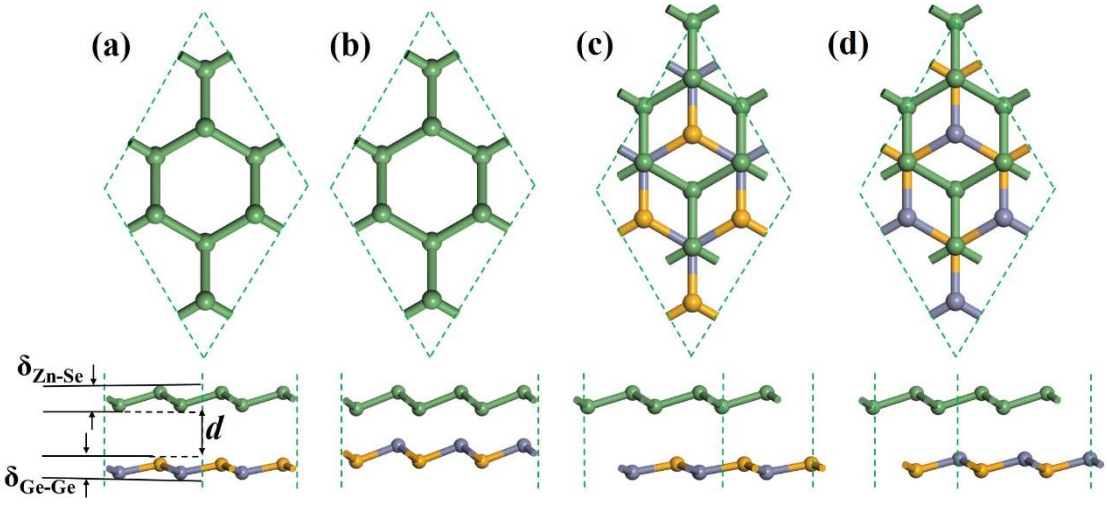

Fig. 1. Top and side view of the atomic model of the germanene/ZnSe heterobilayer: (a) Pattern AAI, (b) Pattern AAII, (c) Pattern ABI, (d) Pattern ABII. The $d, \delta_{\text{Ge-Ge}}$, and $\delta_{\text{Zn-Se}}$ are interlayer distance, buckling height of the germanene and ZnSe respectively. The Zn and Se atom of ZnSe, and Ge atoms in upper/lower level are represented by grey, orange and green balls respectively.

To evaluate the thermal stability of germanene/ZnSe heterobilayers, the *ab-initio* molecular dynamics (AIMD) simulations were performed at 310K. The snapshots of geometric structures at the end of the AIMD simulations for the heterobilayers is presented in Fig.2 (a). The AIMD simulation reveals that the structure of germanene/ZnSe heterostructure is well kept in its original configuration at the temperature of 310K, which demonstrates the heterobilayers can maintain stability at 310K, which is larger than the room temperature. To reveal the binding mechanism, the band structures of pristine germanene, ZnSe and germanene/ZnSe heterostructure are shown in Fig.2 (b). The calculated direct band gap of freestanding ZnSe layer at the PBE level is 2.547 eV with both the conduction band minimum (CBM) and valence band maximum (VBM) located at Γ point in the Brillouin zone (BZ). For pristine germanene, it exhibits gapless semi-metal nature due to the filled state and empty state

bands touched at the high-symmetry point M point of the BZ in this case. Obviously, the band structure of germanene/ZnSe heterobilayers seems to be a simple sum of each constituent, and the direct band gap of 0.503 eV with both CBM and VBM also located at the same Γ point in the BZ. Remarkably, it is noted that a large band gap of 0.503 eV obtained which is much larger than those of silicone/silicane (44-61 meV) and germanene/germanane (82-120 meV) heterostructures. [14,15] Besides, Zhang *et al*. demonstrated that half-hydrogenation breaks the π-bonding network of pristine silicene, resulting in the electrons in the unsaturated Si atoms localized and unpaired, and thus it exhibits ferromagnetic semiconducting with an opened band gap of 0.95 eV.[42] However, according to Wu *et al*.,[43] the experiment reveals that the H_2 plasma treatment need quick kinetics and produce large-area defects after short plasma exposures. Also, the hydrogen-functionalized systems are unstable and easy oxidation under ambient condition. Therefore, take the potential optoelectronic application into consideration, our results demonstrate that single-layer ZnSe can be served as a moderate substrate for germanene. Besides, it is well known that the band gaps of semiconducting materials are usually systematically underestimated by GGA-PBE function due to the nonempirical GGA functional that contains no Hartree-Fock (HF) exchange. Fortunately, Hybrid density functionals, which includes a certain amount of HF exchange that can partially correct for electron-delocalization errors inherent to GGA exchange-correlation functionals and thus further improve upon the GGA results. [32,44] For example, Jochen *et al*. reported that Heyd-Scuseria-Ernzerhof (HSE) exhibits significantly smaller errors than pure density functional theory (DFT) calculations on electronic properties,[45] which make HSE an attractive choice for calculations of semiconductors. Therefore, the more accurate electronic properties could be calculated via implement hybrid density functional theory or the many-body perturbation theory. The direct band gap of single-layer ZnSe at the HSE06 functional is ~3.184 eV (see Fig.2 (c)) with the VBM and CBM located at the same Γ point in the BZ, which is

smaller than the reported values of 3.40 eV [26] and experimental (~3.50 eV) [23]. Such discrepancy is believed to be caused by different modules of the software package we used. The calculated band gap of the germane/ZnSe heterostructure at the HSE06 functional is 0.743 eV (Fig.2c). The result demonstrates that the HSE06 only enlarge the band gap, but the character of electronic properties of germanene/ZnSe heterostructure does not affected as in the PBE level. Since the presence of a finite E_g without degrading electronic properties of germanene is highly expected, the excellent structural stability of heterostructure is a promising candidate for building FETs. Meanwhile, the opened band gap of AAii-stacking is more pronounced than that of the room temperature thermal scale (26meV), suggesting that the on-off current ratio in logical devices made of germanene/ZnSe heterostructure would be largely improved.

To explore the interaction mechanism between germanene and single-layer ZnSe, the total and atom projected density of states (DOS and PDOS) of AAii-stacking is plotted in Fig. 2 (d). It can be seen that electronic states in characteristic peak of the valence bands (~-1.0 eV) and conduction bands around the Fermi level are mainly contributed by germanene, while the peak in the valence bands (< -1.0 eV) is primarily dominated by single-layer ZnSe. Besides, the Ge p and Se p orbitals share the similar states around -1 eV in the valence bands and in the range of 3 to 4 eV in the conduction bands, which are far away from the Fermi level, suggesting the presence of orbital hybridization between germanene and ZnSe substrate. Therefore, we concluded that the germanene and ZnSe are bounded to each other via orbital hybridization.

To better understanding the interaction mechanism between germanene and ZnSe layers, the charge density difference (CDD) of the AAII pattern is calculated. The charge density difference (CDD) of AAII pattern is performed based on the following equation: $\Delta\rho = \rho_{heterostructure} - \rho_{ZnSe} - \rho_{germanene}$, where $\rho_{heterostructure}$, ρ_{ZnSe}, $\rho_{germanene}$ are the total charge densities of the AAii-stacking, single-layer ZnSe and germanene, respectively. As shown in Fig.3 (a), the blue color represents charge accumulation,

while the yellow color represents charge depletion. The charge analysis was determined by the Hirshfeld method. It can be seen that the charge rearrangement localized at the interlayer region, which is the result of orbital overlaps from the Fig.3 (a). The charge depleted on the ZnSe layer and lower Ge atoms, while a large number of charge accumulated at the interlayer region and upper Ge atoms. The Hirshfeld charge analysis shows that the charge transfer of AAII pattern is -0.036 e, with germanene acts as an electron acceptors derived from ZnSe substrate. To get a further insight into the nature of bonding between germanene and ZnSe layer, the electron localization function (ELF) of AAII pattern is calculated. As shown in Fig.3 (b), the grades of ELF are characterized by a color scheme in which red shows that the electrons are highly localized and blue corresponds to the electrons with non-localized.[46] The ELF for AAII pattern is close to one in the interlayer regions suggesting the electrons are paired to form covalent bonds between Ge and Zn or Se atoms. The results demonstrate that the germanene and single-layer ZnSe in AAII pattern are bounded to each other *via* orbital hybridization, which is the reason for large binding energy.

Besides, the corresponding electronic band structure, DOSs, and charge density distributions of AAi, ABi and ABii are also calculated and plotted in Fig. S1 (ESI). The AAI, ABI and ABII heterostructures also show a direct band gap, with the value of 0.287, 0.053 and 0.249 eV, respectively, with both the CBM and VBM being located at the same M point in BZ. Comparing with the partial DOSs of AAi- and ABi-stacking, it can be seen that the CBM near the Fermi level is donated by the Ge p orbital. Therefore, the germanene and single-layer ZnSe in AAI and ABI patterns are paired to each other by the van der Waals (vdW) interaction. Furthermore, the charge density distributions of AAI pattern shows that the charge accumulation on the lower germanene while depletion on the germanene. For the ABI pattern, the charge accumulated on the germanene and at the interlayer region, whereas depleted on the single-layer ZnSe. As a result, germanene acts as charge acceptors and receives 0.019

e from ZnSe substrate, respectively. Such a limited charge transfer is consistent with the moderate binding energy. However, for the ABII pattern, the CBM is contributed by the Se p and Ge p orbitals from the electronic densities of states (DOS) analysis, indicating the slight orbital hybridization. It is worth to be noted that the orbital hybridization between germanene and ZnSe substrate is rather weak, thus incapable of chemical bond forming between the two layers. The charge density difference of ABII pattern shows that charge accumulation on the ZnSe and interlayer regions, whereas charge depletion on the germanene and interlayer regions. The total amount of charge

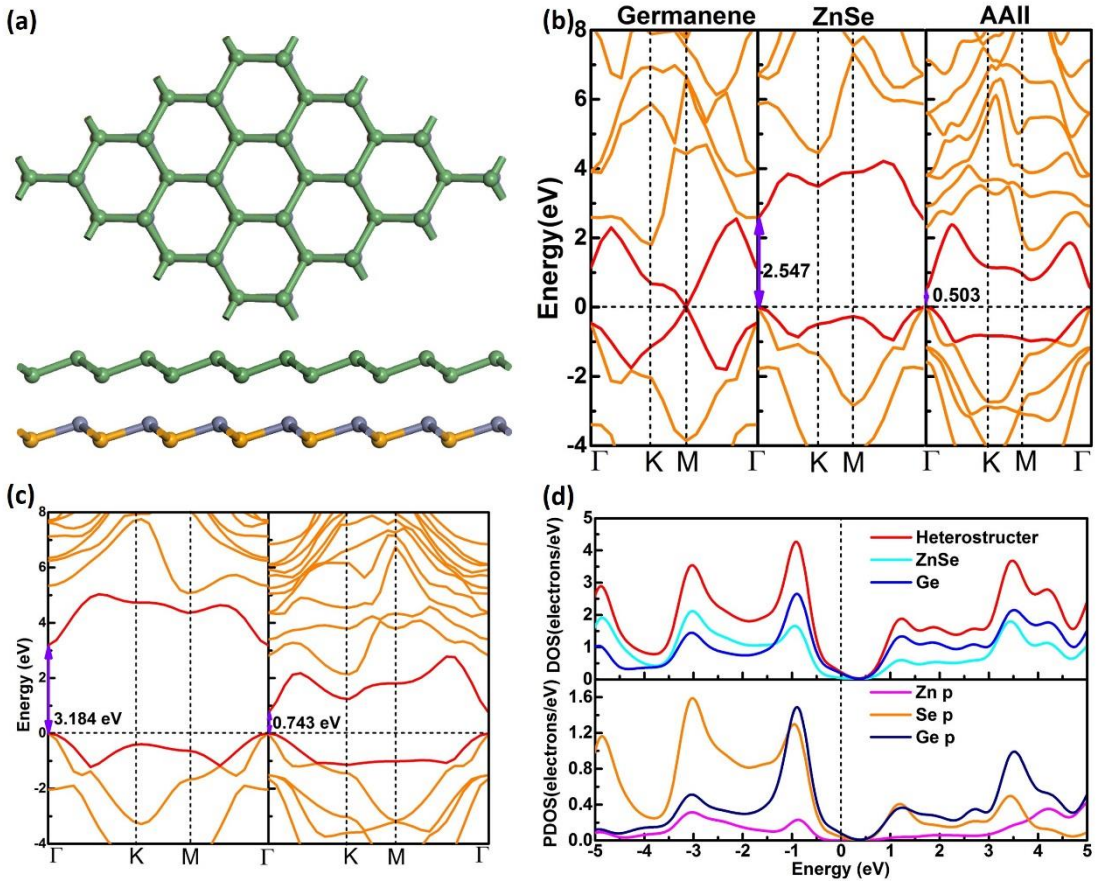

transfer is 0.015 e from single-layer ZnSe to germanene.

Fig.2. (a) Snapshots of the heterobilayers at 310K at the end of 5 ps AIMD simulations. (b) Electronic band structures of germanene, single-layer ZnSe, and AAii-stacking. c) Energy band structure of single-layer ZnSe and AAii-stacking calculated by HSE06. (d) DOS and PDOS of the AAii-stacking configuration. The Fermi level is set to zero and

represented by the black dashed line.

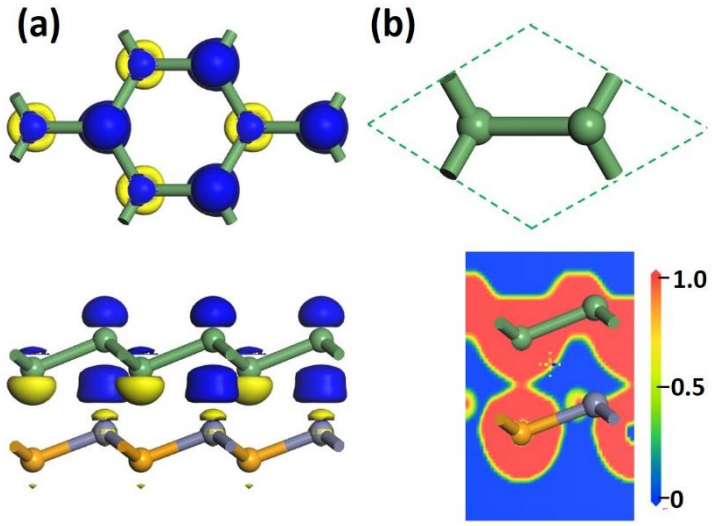

Fig.3. Top and side view of (a) charge density difference and (b) the isosurface of the electron localization function of the ABI pattern configuration. The isosurface refer to isovalues of 0.02 e $Å^{-3}$.

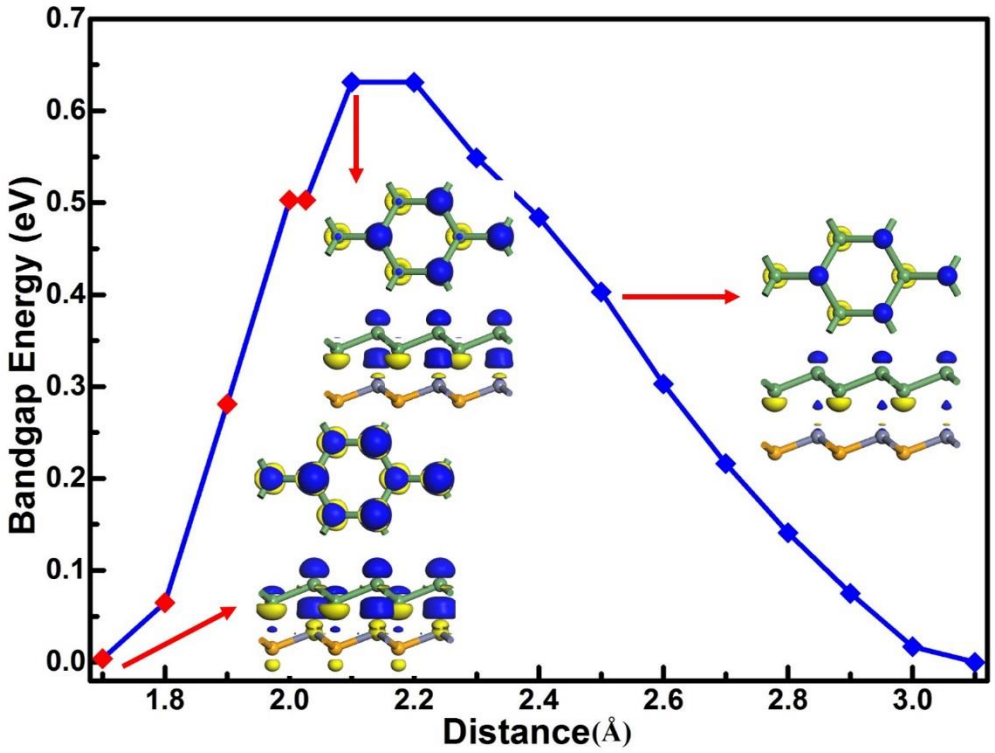

Fig. 4. Variation of the energy bandgap of germanene/ZnSe superstructure as a function of the interlayer distance between the two lattices. The red (blue) dots in the curve indicate the direct (indirect) band gap. The inset is the charge density difference at different distance in the three configurations. The yellow (blue) indicates the charge

depletion (accumulation). Isovalues is 0.02 e $Å^{-3}$.

Some works reported that regulating the interlayer distance (*d*) is a simple way of tuning the electronic structures. [47,48,49] For exploring the relationship between interlayer distance and electronic structure, we changed the interlayer distance and calculated the corresponding band gap, as shown in Fig.4. The results indicate that the band gaps are very sensitive to the interlayer distance. These *d* values are within the sum of covalent radii of Ge-Zn (2.39 Å) and Ge-Se (2.37 Å), indicating that the bond between these atoms is formed. When the interlayer distance decreases, the charge accumulation between Ge and Zn atoms, suggesting the strong orbital hybridization between two layers. Therefore, when the distance is small enough, the orbital hybridization will take up the dominant status, which makes charge distribution in germanene. In this case, the band gap linearly increases with the increasing of interlayer distance from 1.7 to 2.1 Å. On the contrary, when the interlayer distance is relatively large, there is nearly no charge accumulation in the interspace of Ge and ZnSe layers. Therefore, the onsite energy difference of germanene is small and the van der Waals interaction will play a major role in the system, which can induce the inhomogeneous on-site energy of Ge atoms in germanene. In this case, the band gap decreases with the increase of *d*. As shown in Fig.4, when the *d* increased from 2.1 to 3.1 Å, the band gap linearly decreases, and finally diminish at the energy level of 3.1 Å. When the *d* is in the range of equilibrium state (2.026 Å), the band gap reaches a maximum value due to the complementation of orbital hybridization and vdW interaction between germane and ZnSe substrate. We found that when interlayer distance is less than 1.7 Å or larger than 3.0 Å, the germanene/ZnSe heterostructure will experience a semiconductor-metal transition. Therefore, compressing the interlayer distance in a certain range is a simple way of tuning the electronic structures of germanene/ZnSe heterostructure.

Appling an external electric field (E-field) has been recognized as one of the efficient methods to modify or tune the electronic properties of 2D materials. [50,51,52] The

underlying modulation mechanism lies on the giant Stark effect, which is shifting and splitting of spectral lines of atoms due to presence of an external electric field and thus eventually tune 2D materials' electronic structure. A vertical electric field can lead to doping, especially in the case of bilayers it can induce charge transfer between layers. For example, Chu *et al*. showed a continuous band-gap tuning in bilayer MoS_2 with applied gate voltage.[53] Meanwhile, electronic band engineering is still experimentally meaningful,[54] and thus we next investigate the influence of an external uniform electric field on the band gap of heterobilayer. Fig.5 shows the band gap of germanene/ZnSe heterobilayer as a function of vertical E-field magnitude. Two orientations of E-field (+z, -z) along the normal direction of the infinite heterobilayer plane were adopted. The positive direction of the E-field is denoted by the arrows as shown in Fig.5 (c). Interestingly, we note that the band gap natures of AAII pattern is completely independent of the external E-field (Fig.5 (a)). When the E-field reaches -0.001 a.u., the VBM remains at the Fermi level, while the CBM shifts down along the direction of energy reduction with increased E-field, leading to the band gap amounting to 0.617 eV, which is shown in the Fig.5 (b). When the strength of E-field further increased, the band gap falls down rapidly with the increasing intensity of negative external E-field till disappears under E-field at -0.004 a.u., resulting in a semiconductor-to-metal transition. When a positive E-field is applied, the band gap decreases monotonically with the increase of the E-field. The band gap decreases rapidly to 0.359 eV under an E-field of 0.001 a.u. After further increasing the E-field to 0.003 a.u., the band gap reduces to zero and correspondingly experience a semiconductor-to-metal transition. It is well known that the origin of band gap modulation under an external applied E-field is ascribe to the Stark effect. More explicitly, the external E-field could induce an electrostatic potential difference between germanene and ZnSe substrate, leading to the energy levels of two layers would be separated from each other, causing a shifting of energy levels and thus changing the band gap. With increasing magnitude of E-field, the energy

level shifting becomes more and more pronounced and finally leads to a semiconductor-to-metal transition. Therefore, the band gap can be efficiently modulated by the external E-field, and the transition is easily achieved.

Except for the tunable band gap, the applied E-field can substantially enhance the interaction between individual single-layers and continuously modulate electron redistribution at the interface.[55,56,39] Inspired by these reports, for a closer look on the underlying mechanism of the band gap affected by external E-field, the changes in the charge transfer and binding energy as a function of the E-field are calculated and plotted in Fig.5 (d). The positive Q means charge transfer from single-layer ZnSe to germanene, and the more negative binding energy indicates the heterobilayer is more stable. It is clearly seen that charge transfer exhibiting a linear behavior within the E-field range of -0.004 to 0.003 a.u. When the E-field is applied in the positive direction, the charge transfer from ZnSe substrate to germanene decreases linearly with the increase of the E-field strength, and thus germanene is more positively charged. The charge transfer increases to -0.072 e upon increasing the E-field to 0.003 a.u. In sharp contrast, the charge transfer increases gradually with the increase of the E-field strength in the negative direction. When the E-field increases to -0.002 a.u., single-layer ZnSe no longer donates electrons to germanene, and more and more charges begin to transfer from germanene to ZnSe substrate. The charge transfer reaches the maximum value of 0.015 eV when the strength of E-field is -0.004 a.u. Most interestingly, the binding energy decreases with increasing strength of the E-field. The binding energy decreases to the minimum value of -0.809 eV upon increasing the E-field to -0.004 a.u. Because the charge transfer between heterogeneous layers which is initiated by an applied external E-field, enhancing the interlayer electrostatic interaction, and the binding energy of heterobilayers becomes more and more negative correspondingly. These results demonstrate that the interaction between germanene and ZnSe substrate can be effectively modulated by applying appropriate external E-field.

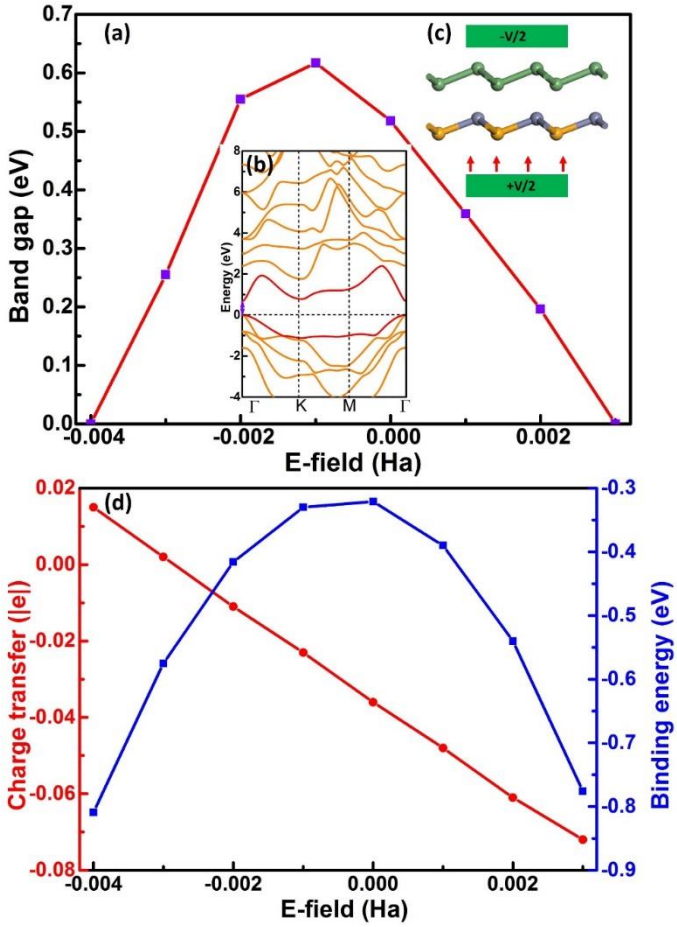

Fig.5. (a) The calculated energy band gap as a function of E-field for ABI pattern, (b) Band structure of AAII pattern at the E-field of -0.001 a.u., (c) The positive direction of the E-field is pointed by the red arrows from ZnSe to germanene, and (d) the binding energy and charge transfer of the AAii-stacking structure as a function of E-field.

Another promising route towards a continuous band gap is elastic strain engineering. For example, strain-engineering [57] of Si, SiGe, Ge has been successfully used in the semiconductor industry to impressively improve the performance levels of conventional metal-oxide-semiconductor field-effect transistors (MOSFETs), and mechanical strain can be seen as a solution for higher carrier mobility in nano MOSFETs. The band gap tuned by strain engineering due to the energy bands (levels) around the Fermi level are very vulnerable to orbital coupling or interaction with neighboring atoms within the crystal, and the amount of strain strongly depended on

the degree of orbital interaction.[58] In this section, we investigated the evolution of the electronic band structures of heterobilayer when it is subjected to external tensile and compressive strain by changing the lattices as $\varepsilon_2 = (a - a_0)/a_0$, where a and a_0 are the strained and equilibrium lattice constants of the heterobilayer. Moreover, the strain energy is also considered and can be expressed as $\Delta E = E_d - E_p$, where E_d and E_p are the total energy of deformed and pristine heterobilayer, respectively.

Fig.6 (a) illustrates the strain modulation of the band gap for germanene/ZnSe heterostructure. The electronic band structures can be significantly modulated upon applying in-plane strain on the germanene/ZnSe heterobilayers. For the biaxial compressive strain, the band gap increases rapidly and amounts to the maximum value of 0.673 eV at strain of -1%. And then the band gap decreases monotonically with increasing the compressive strain from -2% (0.613 eV) to -7% (0 eV). For the uniaxial compressive strain, different from the biaxial compressive strain, the electronic band gaps increase firstly by increasing the strain from 0 to -3%, and then start to reduce. It is noted that the band gap can be continuously tuned from 0.553 (-2% strain) to 0 eV (-7% strain) by increasing the uniaxial compressive strain from -2 to -7%, which exhibits linearly decrease relationship. In sharp contrast, the band gap decreases monotonically with the increase of tensile strain from 0 to 5% both under the uniaxial and biaxial strain. The application of uniaxial tensile strain gradually lower the band gap from 0.389 (1% strain) to 0 eV (5% strain). Similar to the case of uniaxial tensile strain, the heterobilayers exhibit a linear reduction in the band gap from 0.378 eV (1% strain) to 0 (5% strain) under biaxial tensile strain.

In order to better understanding the above results, the strain energy as a function of external strain is plotted in Fig.6 (b). It is found that the strain energy increases monotonously with the increasing of mechanical strain within the range of -7 to 5% both under uniaxial and biaxial strain, which suggests that the strain is in the range of elastic deformation so that the deformed structure can be restored to its initial state

when mechanical strain is removed. Thus, the germanene/ZnSe heterobilayer will be used as a candidate configuration for pressure sensor, and the variation of band gaps is independent of the distribution of biaxial strain. Therefore, applying external strain is a simple way of modulating the electronic structure of germanene/ZnSe heterostructure.

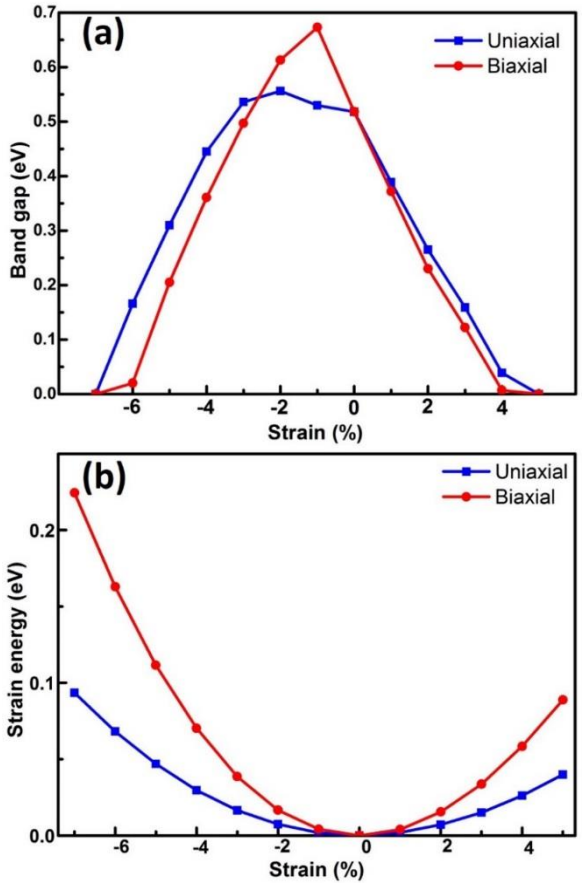

Fig.6. (a) Variation of the bandgap and (b) the strain energy of the AAii-stacking structure as a function of mechanical strain.

To further understand the electronic charge reorganization and explore the potential application in future optoelectronics such as field-emitting devices, the work function of individual germanene, ZnSe and heterobilayer structure are calculated. The work function is usually used to describe the minimum required energy to remove an electron from the interior of a solid to the surface. For a given surface, it is defined by, $\phi_\omega = -e\phi_0 - E_F$, where $-e$ is the charge of an electron, ϕ_0 is the electrostatic potential in a vacuum away from the surface, and E_F is the energy of the Fermi level. The

calculated WF of individual germanene is found to be 4.41 eV, which is slightly larger than the reported value (4.19 eV) [59] due to different software we used, the value is comparable to that of graphene. [60] The WF of the single-layer ZnSe is 5.68 eV. After the two single layers are paired together in AAii-stacking, the WF of heterostructure is 4.95 eV which is 0.54 eV higher than that of individual germanene. It is reasonable to think that the occurrence of orbital hybridization between the germanene and ZnSe substrate, which increases the WF of germanene and meanwhile decreases that of ZnSe layer, supporting the above calculated DOS and ELF.

For normal incidence and in-plane light polarization, the light absorption spectrum is determined by the imaginary part of the dielectric function and the absorption coefficient of the 2D material. [46] In this section, we will discuss the adsorption coefficient and the imaginary part ε_2 of dielectric function of germanene, ZnSe, and their AAii-stacking heterostructure. As shown in Fig. 7, it is seen that both the dielectric function and adsorption coefficient of the AAII pattern have changed greatly in comparison with those of the individual germanene and ZnSe. Firstly, we discuss the dielectric function based on its imaginary part, which is related to the inter-band transitions, as plotted in Fig. 7 (a). For germanene, the highest peak at around 1 eV is ascribed to the π-π^* transition states located at *k* points near the BZ boundary along the K-M direction.[61] For ZnSe substrate, the edge of the first peak extends to 2.5 eV due to its large band gap. The first peak locates around 3.2 eV, indicating that single-layer ZnSe can only absorb ultraviolet light (>3 eV). However, for the germanene/ZnSe heterostructure, the edge of first peak appears at the energy level of 1.4 eV, indicating that the heterobilayer can absorb visible light. Expectedly, it can be seen that the first peak appears at the energy level of 2.2 eV, corresponding to the yellow-blue region (2.0~2.85 eV), which is the mainly strong intensity of the sunlight. Thus, the heterobilayer with tunable bandgap can be more advantageous as light-absorbing materials for optoelectronic application. Furthermore, it is noted that the ε_2 values of

the dielectric function of the heterostructure are much higher than that of the individual germanene and ZnSe substrate in the energy region, which shows the remarkable enhanced abilities to adsorb photons. Therefore, more photons in visible light region (1.5~3.0 eV) can be adsorbed by the germanene/ZnSe heterostructure.

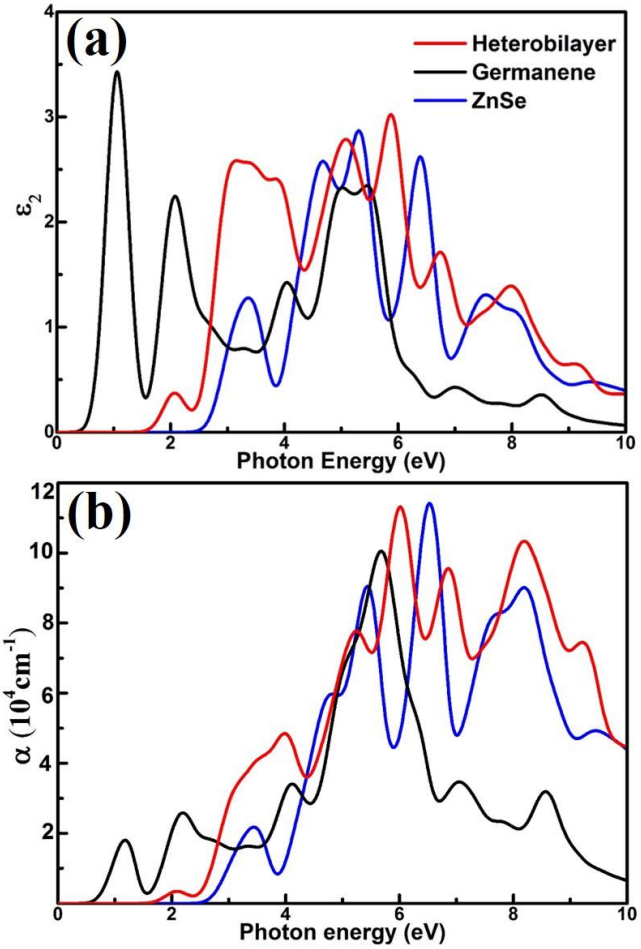

Fig.7. (a) Imaginary part of dielectric function and (b) adsorption coefficient of germanene, ZnSe, and germanene/ZnSe heterostructure for the polarization vectors parallel to the two dimensional plane.

In order to better understanding the optical properties, the adsorption coefficients with polarization vectors parallel to the layers plane for heterostructure is shown in Fig. 7 (b). The decay of light intensity spreading in a unit length of medium is defined as the absorption coefficient. It is clear that the adsorption coefficient of the heterobilayer

is stronger than the individual germanene and ZnSe substrate, implying that the heterobilayer has extraordinary light harvesting ability in the entire visible wavelength range. Which is in good agreement with a broad-gap to narrow-gap transition observed in single-layer ZnSe, suggesting that the optical properties of heterostructure are superior to those of individual layer. Owing to the electrons can be directly excited from the valence band of the bottom layer to the conduction band of top layer of heterobilayer, a distinct redshift of the absorption spectrum edge can be observed in comparison with that of the freestanding ZnSe substrate. In contrast, the calculated adsorption coefficients of the heterostructure corresponding to the individual germanene shows a hypsochromic shift around 0.5 eV of the adsorption edge. Generally, the germanene/ZnSe heterobilayer adsorbs considerable light over the entire sunlight spectrum and even in the infrared light region (<1.6 eV) adsorption with the direct band gap, indicating the potential application in solar cells. It can be seen the germanene/ZnSe heterobilayers holds the typical optical characteristics of individual ZnSe substrate and germanene and also exhibits some unique optical properties, such as the unique dielectric function and absorption spectrum in the visible light irradiation range, which shows great potential applications in optical transmission and photoelectric devices.

4. Conclusion

In summary, we have performed systemic investigation on the structural, electronic and optical properties of the germanene, single-layer ZnSe substrate and their heterobilayer structures based on DFT-D computations. Different from the individual germanene with zero-gap and single-layer ZnSe of wide direct-gap, the germanene/ZnSe heterobilayer structure is found to be a direct-gap semiconductor with an electronic band of 0.503 eV with stable structure at room temperature. Moreover, the opened band gap can be further modulated by the interlayer distance between the two layers. In addition, the effects of an applied out-of-plane electric field and biaxial

strain on the electronic of the heterobilayer were also studied. These findings demonstrate that the single-layer ZnSe can serve as a moderate substrate for germanene. We also found that the germanene/ZnSe heterostrcuture is very promising for high performance nano-electronic applications due to its tunable bandgaps via applying vertical electric field. More interestingly, external mechanical strain is also a simple way of tuning the electronic properties of the heterobilayer and a semiconductor-to-metal transmission can be observed. Furthermore, the heterobilayer exhibits some unique optical properties and strong visible and infrared light absorption from the dielectric function and absorption coefficient analysis. Therefore, the germanene/ZnSe heterostructure is a promising 2D semiconductor with high potential for novel applications in nano-electronics and opto-electronics, such as field-effect transistors (FETs) at room temperature and strain sensors.

Author Information

Corresponding authors

E-mail: xianpingchen@cqu.edu.cn.

Acknowledgements

This work was supported by the National Natural Science Foundation of China under Grant No. 51706029 and the Fundamental Research Funds for the Central Universities under Grant 106112017CDJQJ128836.

Reference

1 M. Xu, T. Liang, M. Shi and H. Chen, *Chem. Rev.*, 2013, **113**, 3766–3798.

2 A. Kuc, N. Zibouche and T. Heine, *Phys. Rev. B*, 2011, **83**, 245213.

3 J. A. Yan, S. P. Gao, R. Stein and G. Coard, *Phys. Rev. B - Condens. Matter Mater. Phys.*,2015,**91**,245403.

4 S. Zhang, Z. Yan, Y. Li, Z. Chen and H. Zeng, *Angew. Chemie - Int. Ed.*, 2015, **54**, 3112–3115.

5 M. Zhou, X. W. Lou and Y. Xie, *Nano Today*, 2013, **8**, 598–618.

6 Y. Zhu, S. Murali, M. D. Stoller, K. J. Ganesh, *Science*, 2011, **332**, 1537–41.

7 J. Dai, Z. Li, J. Yang and J. Hou, *Nanoscale*, 2012, **4**, 3032.

8 L. Liu, J. Zhang, J. Zhao and F. Liu , *Nanoscale*, 2012, **4**, 5910.
9 K. S. Novoselov, A. K. Geim, S. V Morozov, D. Jiang, Y. Zhang, S. V Dubonos, I. V Grigorieva and A. A. Firsov, *Science*, 2004, **306**, 666–9.
10 Y. Wang, Z. Ni, Q. Liu, R. Quhe, J. Zheng, M. Ye, D. Yu, J. Shi, J. Yang, J. Li and J. Lu, *Adv. Funct. Mater.*, 2015, **25**, 68–77.
11 M. Ye, R. Quhe, J. Zheng, Z. Ni, Y. Wang, Y. Yuan, G. Tse, J. Shi, Z. Gao and J. Lu, *Phys. E Low-Dimensional Syst. Nanostructures*, 2014, **59**, 60–65.
12 A. Nijamudheen, R. Bhattacharjee, S. Choudhury and A. Datta, *J. Phys. Chem. C*, 2015, **119**, 3802–3809.
13 A. K. Geim and K. S. Novoselov, *Nat. Mater.*, 2007, **6**, 183–191.
14 R. Zhang, C. Zhang, W. Ji, F. Li, M. Ren, P. Li, M. Yuan and P. Wang, *Phys. Chem. Chem. Phys.*, 2015, **17**, 12194–12198.
15 R. W. Zhang, C. W. Zhang, W. X. Ji, S. J. Hu, S. S. Yan, S. S. Li, P. Li, P. J. Wang and Y. S. Liu, *J. Phys. Chem. C*, 2014, **118**, 25278–25283.
16 C. C. Liu, W. Feng and Y. Yao, *Phys. Rev. Lett.*, 2011, **107**, 076802.
17 P. Vogt, P. De Padova, C. Quaresima, J. Avila, E. Frantzeskakis, M. C. Asensio, A. Resta, B. Ealet and G. Le Lay, *Phys. Rev. Lett.*, 2012, **108**, 155501.
18 Y. P. Wang, W. X. Ji, C. W. Zhang, P. Li, F. Li, P. J. Wang, S. S. Li and S. S. Yan, *Appl. Phys. Lett.*, 2016, **108**, 073104.
19 C. Si, J. Liu, Y. Xu, J. Wu, B. L. Gu and W. Duan, *Phys. Rev. B - Condens. Matter Mater. Phys.*, 2014, **89**, 115429.
20 Y. P. Wang, W. X. Ji, C. W. Zhang, P. Li, F. Li, M. J. Ren, X. L. Chen, M. Yuan and P. J. Wang, *Sci. Rep.*, 2016, **6**, 20342.
21 S. J. Zhang, C. W. Zhang, S. F. Zhang, W. X. Ji, P. Li, P. J. Wang, S. S. Li and S. S. Yan, , *Phys. Rev. B*, 2017, **96**, 205433.
22 H. Zhao, C. W. Zhang, W. X. Ji, R. W. Zhang, S. S. Li, S. S. Yan, B. M. Zhang, P. Li and P. J. Wang, , *Sci. Rep.*, 2016, **6**, 20152.
23 Y. Sun, Z. Sun, S. Gao, H. Cheng, Q. Liu, J. Piao, T. Yao, C. Wu, S. Hu, S. Wei and Y. Xie, , *Nat. Commun.*, 2012, **3**, 1057.
24 J. Zhou, B. G. Sumpter, P. R. C. Kent and J. Huang, *ACS Appl. Mater. Interfaces*, 2015, **7**, 1458–1464.
25 C.-J. Tong, H. Zhang, Y.-N. Zhang, H. Liu and L.-M. Liu, *J. Mater. Chem. A*, 2014, **2**, 17971–17978.
26 L. Li, P. Li, N. Lu, J. Dai and X. C. Zeng, , *Adv. Sci.*, 2015,**2**,12.

27 X. Chen, C. Tan, Q. Yang, R. Meng, Q. Liang, M. Cai, S. Zhang and J. Jiang, , *J. Phys. Chem. C*, 2016,**120**,13987-13994.

28 L. Kou, T. Frauenheim and C. Chen, *J. Phys. Chem. Lett.*, 2014, **5**, 2675–2681.

29 J. Perdew, K. Burke and M. Ernzerhof, *Phys. Rev. Lett.*, 1996, **77**, 3865–3868.

30 S. Grimme, , *J. Comput. Chem.*, 2006, **27**, 1787–1799.

31 J. Tao, J. P. Perdew and A. Ruzsinszky, *Proc. Natl. Acad. Sci. U. S. A.*, 2012, **109**, 18–21.

32 S. I. Allec and B. M. Wong, *J. Phys. Chem. Lett.*, 2016, **7**, 4340–4345.

33 J. Heyd, G. E. Scuseria and M. Ernzerhof, *J. Chem. Phys.*, 2003, **118**, 8207–8215.

34 M. D. Segall, P. J. D. Lindan, M. J. Probert, C. J. Pickard, P. J. Hasnip, S. J. Clark and M. C. Payne, *J. Phys. Condens. Matter*, 2002, **14**, 2717–2744.

35 J. Jiang, Q. Liang, R. Meng, Q. Yang, C. Tan, X. Sun and X. Chen, *Nanoscale*, 2017, **9**, 2992–3001.

36 G. Satta, G. Cappellini, M. Palummo and G. Onida, *Science*, 2001, vol. 22, pp. 78–80.

37 S. Saha, T. Sinha and A. Mookerjee, *Phys. Rev. B*, 2000, **62**, 8828–8834.

38 J. C. Garcia, D. B. De Lima, L. V. C. Assali and J. F. Justo, *J. Phys. Chem. C*, 2011, **115**, 13242–13246.

39 Y. Ding and Y. Wang, *Appl. Phys. Lett.*, 2013,**103**,043114.

40 Y. Ma, Y. Dai, M. Guo, C. Niu and B. Huang, *Nanoscale*, 2011, **3**, 3883–3887.

41 M. Houssa, B. van den Broek, E. Scalise, G. Pourtois, V. V. Afanas'ev and A. Stesmans, *Phys. Chem. Chem. Phys.*, 2013, **15**, 3702.

42 C. W. Zhang and S. S. Yan, *J. Phys. Chem. C*, 2012, **116**, 4163–4166.

42 J. Wu, L. Xie, Y. Li, H. Wang, Y. Ouyang, J. Guo and H. Dai, *J. Am. Chem. Soc.*, 2011, **133**, 19668–19671.

43 J. Wu, L. Xie, Y. Li, H. Wang, Y. Ouyang, J. Guo and H. Dai, *J. Am. Chem. Soc.*, 2011, **133**, 19668–19671.

44 S. I. Allec, N. V. Ilawe and B. M. Wong, *J. Phys. Chem. Lett.*, 2016, **7**, 2362–2367.

45 J. Heyd and G. E. Scuseria, *J. Chem. Phys.*, 2004, **121**, 1187.

46 X. Chen, Q. Yang, R. Meng, J. Jiang, Q. Liang, C. Tan and X. Sun, *J. Mater. Chem. C*, 2016, **4**, 5434–5441.

47 L. Li and M. Zhao, *Phys. Chem. Chem. Phys.*, 2013, **15**, 16853.

48 X. Chen, X. Sun, J. Jiang, Q. Liang, Q. Yang and R. Meng, *J. Phys. Chem. C*, 2016, **120**, 20350–20356.

49 S. Li, C. W. Zhang, S. S. Yan, S. J. Hu, W. X. Ji, P. J. Wang and P. Li, , *J. Phys. Condens. Matter*, 2014, **26**, 395003.
50 Q. Liang, J. Jiang, R. Meng, H. Ye, C. Tan, Q. Yang, X. Sun, D. Yang and X. Chen, *Phys. Chem. Chem. Phys.*, 2016, **18**, 16386–16395.
51 Y. Zhang, T. T. Tang, C. Girit, Z. Hao, M. C. Martin, A. Zettl, M. F. Crommie, Y. R. Shen and F. Wang, graphene, *Nature*, 2009, **459**, 820–823.
52 Q. Tang, J. Bao, Y. Li, Z. Zhou and Z. Chen, *Nanoscale*, 2014, **6**, 8624–8634.
53 T. Chu, H. Ilatikhameneh, G. Klimeck, R. Rahman and Z. Chen, *Nano Lett.*, 2015, **15**, 8000–8007.
54 S. Zhang, N. Wang, S. Liu, S. Huang, W. Zhou, B. Cai, M. Xie, Q. Yang, X. Chen and H. Zeng, *Nanotechnology*, 2016, **27**, 274001.
55 N. Gao, J. C. Li and Q. Jiang, *Phys. Chem. Chem. Phys.*, 2014, **16**, 11673–11678.
56 M. L. Lee, E. A. Fitzgerald, M. T. Bulsara, M. T. Currie and A. Lochtefeld, *J. Appl. Phys.*, 2005, **97**, 11101.
57 S. Yang, S. Tongay, Y. Li, Q. Yue, J.-B. Xia, S.-S. Li, J. Li and S.-H. Wei, *Nanoscale*, 2014, **6**, 7226.
58 H. Sahin and F. M. Peeters, *Phys. Rev. B - Condens. Matter Mater. Phys.*, 2013, **87**, 085423.
59 G. Giovannetti, P. A. Khomyakov, G. Brocks, V. M. Karpan, J. Van Den Brink and P. J. Kelly, *Phys. Rev. Lett.*, 2008, **101**, 026803.
60 F. Bechstedt, L. Matthes, P. Gori and O. Pulci, *Appl. Phys. Lett.*, 2012, **100**, 261906.